https://doi.org/10.5194/egusphere-2026-4327
Preprint. Discussion started: 17 August 2026

Why has flood risk increased in a millennia-old mountainous town? Engineering-induced transformation of compound flood pathways in Baifusi, China

Hairun Shu[1,2], Yi Liu[1,2], Jun Guo[1,2], Miao Xiao[1,2], and Zhenhan Deng[1,2]

1 School of Civil and Hydraulic Engineering, Huazhong University of Science and Technology, 1037 Luoyu Road, Wuhan, Hubei 430074, People's Republic of China

2 The Hubei Province Key Laboratory of Digital Valley Science and Technology, Huazhong University of Science and Technology, 1037 Luoyu Road, Wuhan, Hubei 430074, People's Republic of China

Correspondence to: Yi Liu (Prof_liuyi@hust.edu.cn)

Abstract. Baifusi, a long-inhabited mountain-river town in China, coexisted with floods, yet damaging inundation has become concentrated in the recent engineering era. This study asks why flood risk has risen markedly over the last decade. We combine hydrological monitoring, field floodmarks, historical satellite images, drainage calculations, reservoir-operation rule learning, operation logs, surveyed terrain reconstruction, one-dimensional–two-dimensional coupled hydrodynamic scenario modelling, threshold analysis and interpretable surrogate-model evidence. The evidence shows that rainfall magnitude alone is insufficient: the 2016 event had a rare 24 h rainfall return period but a moderate flood-peak return period, while the 2023 event combined high Najitan release, Qiedao tributary inflow, Jinlongtan downstream backwater and local drainage blockage. Matched scenarios show a persistent 1.56–2.08 m tributary increment, whereas the downstream-backwater increment decreases from 1.67 m in the 5-year scenario to 0.03 m in the 100-year scenario. Relative to the 357.01 m hospital-entrance threshold, effective protection capacity decreases from about 42 years under the mainstream-only boundary to about 17 years with tributary inflow and 10 years under the full compound boundary. Archival images indicate a shift from sparse riverfront occupation in 2009 to a dense riverfront building belt by 2023. Pump-station calculations show that internal drainage capacity is 2.62–3.00 $m^3 s^{-1}$, so ponding and backflow become critical when river stage is high. Flood-risk management in engineered mountain towns should move beyond a single return-period defence standard towards a process-based system that jointly manages upstream releases, tributary timing, downstream stage, drainage outlets and exposure control.

1 Introduction

Mountain towns often develop through a long process of adjustment to local water, terrain, transport, and livelihood conditions. In such settlements, flood risk is not only a hydrological property but also a historical relationship between flood pathways, building locations, riverfront uses, warning practice, and local memory. Baifusi Town is a representative case. It is a long-inhabited ancient town in a mountainous river corridor, with a dense riverfront

https://doi.org/10.5194/egusphere-2026-4327
Preprint. Discussion started: 17 August 2026

settlement, steep surrounding hillslopes, a tributary confluence, and upstream and downstream water-control projects. Local knowledge and historical land use allowed the town to coexist with recurrent floods for a long period, but recent records show a different pattern: inundation has become frequent, damaging, and difficult to explain by rainfall magnitude alone.

The central scientific problem is therefore not whether a numerical model can reproduce one flood map. The problem is why a settlement that had adapted to flooding over centuries now experiences a lower threshold for damaging inundation. This distinction matters for natural hazards research. A model-centred paper would mainly report calibration statistics and inundation depths. A risk-transformation paper must ask how engineered boundaries, drainage pathways, exposure, and social confidence in protection changed the mapping from rainfall and discharge to damage.

Recent flood-risk literature has moved away from single return-period maps toward decision-relevant, high-resolution and threshold-aware analysis. Street-scale or confined-valley decisions require terrain-sensitive hydraulic modelling because small errors in channel geometry, urban elevation, roughness or boundary timing can change whether a street, hospital, bridge approach or drainage outlet is classified as safe or inundated (Bates et al., 2010; Sampson et al., 2015; Bates et al., 2021).

Recent reviews and event-based applications have further emphasized that flood models need credible terrain, boundary conditions and uncertainty treatment when they are used for local decisions (Jafarzadegan et al., 2023; Cea et al., 2024; Khosh Bin Ghomash et al., 2024; Khosh Bin Ghomash et al., 2025).

Remote-sensing and exposure studies also show that hazard maps become more useful when inundation extent is connected to exposed people, buildings and critical infrastructure (Wing et al., 2022; Betterle and Salamon, 2024).

Operational warning and urban response depend on impact-relevant information, including emergency access, road passability and critical infrastructure (Pregnolato et al., 2017; Koks et al., 2019).

Impact-based forecasting and event-fatality analyses further show why rapid water-level detection, warning thresholds and behavioural response matter during short-lead-time floods (Alfieri et al., 2024; Merz et al., 2024; Rhein and Kreibich, 2025). These themes are directly relevant to Baifusi because the town's practical flood threshold is controlled by local street-entry elevations, drainage outlets, reservoir operation and low-lying riverfront occupation.

A second literature stream concerns compound, nonstationary and counterfactual flooding. Compound hazards arise when multiple drivers occur together or in close sequence, and their impact can exceed what would be inferred from any single driver (Zscheischler et al., 2018; Bevacqua et al., 2020; Green et al., 2025).

https://doi.org/10.5194/egusphere-2026-4327
Preprint. Discussion started: 17 August 2026

For flood forecasting and hydraulic diagnosis, this literature emphasizes uncertainty quantification, boundary interactions, and event storylines rather than one deterministic design load (Abbaszadeh et al., 2022; Goulart et al., 2024).

Nonstationary rainfall and flood-frequency studies further show that design values estimated from historical stationarity can understate changing hydroclimatic risk (Bevacqua et al., 2019; Bevacqua et al., 2023; Slater et al., 2021a).

This has direct implications for design rainfall and flood-estimation practice, where nonstationary intensity-duration-frequency and design-flood assumptions increasingly require explicit review (Schlef et al., 2023; Wasko et al., 2024). Observed and projected changes in precipitation extremes and flood damages provide the broader climate context for such nonstationarity, although they do not by themselves explain the Baifusi events (Davenport et al., 2021; Fowler et al., 2021; Huang and Swain, 2022).

At the flood-frequency scale, recent work also warns that historically framed 20-year, 50-year, and 100-year floods should be interpreted cautiously under changing hydroclimatic conditions (Slater et al., 2021b; Montanari et al., 2024).

A third body of work is especially important for this paper: flood-control works can reduce hazard while redistributing residual risk, changing exposure, and altering risk perception. Earlier risk-analysis studies emphasize matching model complexity to the decision and communicating uncertainty rather than treating a mapped return period as a complete safety statement (Apel et al., 2009; Beven, 2006).

Recent syntheses of disastrous floods and unprecedented hydroclimatic events show that protection standards, land-use decisions, and preparedness can become misaligned when climate, river modification, and social exposure co-evolve (Merz et al., 2021; Kreibich et al., 2022; Rhein and Kreibich, 2025; Grodek and Benito, 2025).

Global exposure analyses and human-influence studies similarly indicate that settlement expansion onto flood-prone land can convert residual hazard into repeated losses even where protection exists (Tellman et al., 2021; Rentschler et al., 2022; Mazzoleni et al., 2022).

Settlement-pattern studies add that exposure growth is not socially neutral and can be strongly shaped by where people and assets occupy floodplains under perceived protection (Devitt et al., 2023; Wing et al., 2022).

The paper also responds to a long-standing problem in flood-risk analysis: the level of model detail should match the decision being made (Apel et al., 2009). Large-scale flood hazard models are useful for screening and comparison (Sampson et al., 2015), while local heritage-town management requires street-scale thresholds, validated terrain, boundary timing and explicit treatment of protection-induced exposure.

Regional flood trends can increase or decrease under climate forcing depending on hydroclimatic context (Bloschl et al., 2019). Climate-risk management therefore increasingly emphasizes stakeholder values and deep uncertainty rather than one historical design standard (Keller et al., 2021; Slater et al., 2021a).

This perspective is consistent with recent flood-risk syntheses and design-flood reviews, which recommend adaptive decision pathways when climate, exposure and infrastructure assumptions are no longer stationary (Merz et al., 2021; Wasko et al., 2024). Baifusi is not presented as a globally unprecedented flood case, but as a case where the assumptions behind local protection capacity appear to have become outdated.

A common interpretation of recent flood risk is to attribute the increase to more extreme rainfall. That explanation is plausible in many regions, but the Baifusi evidence indicates that it is incomplete. During the 2023 event, severe town inundation occurred even though the 24 h rainfall return periods estimated for key catchments were moderate rather than exceptional. The Youshui mainstream rainfall return period was about 7.75 years, the Qiedao tributary rainfall return period was about 3.26 years, and the Jinlongtan-area rainfall return period was about 2.96 years. A moderate rainfall event should not, by itself, produce severe inundation if the flood-protection and drainage system retained its historical safety margin. The event therefore points to changed thresholds.

The value of the case is therefore twofold. Empirically, it provides a rare synthesis of flood records, reservoir-operation data, high-resolution terrain correction, one-dimensional–two-dimensional coupled hydraulic modelling, local threshold information, floodmark checks, drainage evidence and interpretable surrogate modelling for a single ancient town. Conceptually, it proposes that flood risk in long-inhabited mountain settlements can undergo engineering-induced risk transformation: protective works and development change flood pathways, resident exposure and the effective threshold at which moderate events become damaging.

This framing is also consistent with land-river interface research, which treats hazard, land use, infrastructure and river processes as interacting components rather than independent domains (Grabowski et al., 2022).

The specific contribution is not a new shallow-water solver or a new design-flood frequency method. It is a multi-boundary attribution and threshold-migration framework for long-inhabited mountain towns whose flood risk is reshaped by reservoir operation, tributary confluence, downstream backwater, levee-drainage interaction, and exposure growth. The framework connects conventional return-period scenarios to observed impact thresholds, thereby showing why a town can become frequently inundated without requiring each damaging event to be an extreme rainfall event.

Methodologically, the study combines field investigation, terrain evidence, one-dimensional–two-dimensional coupled hydrodynamic modelling, reservoir-operation analysis, nested hydraulic-boundary scenarios, and local impact-threshold analysis.

https://doi.org/10.5194/egusphere-2026-4327
Preprint. Discussion started: 17 August 2026

This paper reconstructs those threshold changes through a multi-boundary attribution framework. We combine evidence from historical flood frequency, typical event comparison, reservoir-operation modelling, terrain correction, hydrodynamic scenario experiments, local street-entry thresholds, inundation-area response, and model-validation records. The working hypothesis is that engineering works have both protective and risk-transforming effects. Upstream reservoir regulation reduces flood peaks, but the remaining sustained releases may coincide with tributary inflows and downstream backwater. Levees reduce direct river overflow but can also obstruct mountain runoff and local drainage unless drainage capacity is upgraded at the same time. Meanwhile, perceived safety behind hydraulic structures may encourage settlement and production activities to expand into low-lying hazardous areas.

The objectives are to (1) quantify the reported increase in inundation frequency, (2) test whether recent damaging floods can be explained by rainfall magnitude alone, (3) isolate the contributions of mainstream release, Qiedao tributary inflow, and Jinlongtan backwater to water level and inundation area, (4) translate hydrodynamic results into threshold exceedance and effective protection capacity, and (5) propose a risk-governance framework for ancient mountain towns affected by reservoir groups, tributary confluences, levees, and exposure expansion.

1.1 From return-period design to process-based flood-risk management

Traditional flood-control planning often communicates safety through a design return period. If p is the annual exceedance probability, the return period is defined by Eq. (1). A levee, channel, or reservoir operation rule is then described as meeting a 10-year, 20-year, or 50-year standard. This convention remains useful because it gives engineers and managers a common probabilistic language. However, it can become misleading when town inundation is controlled by interacting boundaries rather than by one design discharge at one cross-section.

$$T = \frac{1}{p} \tag{1}$$

In Baifusi, a return-period label attached to rainfall or mainstream discharge does not uniquely determine impact. A 10-year mainstream boundary may remain below key town thresholds if the tributary and downstream boundaries are weak. A smaller event may become damaging if tributary inflow and backwater coincide with sustained reservoir release. Thus, effective risk is conditional: $P[I > I_{crit} \mid B(t), E]$, where I is an impact indicator, I_{crit} is a street-entry or damage threshold, $B(t)$ denotes the time-varying boundary vector of upstream release, tributary inflow, downstream stage, local rainfall-runoff, and drainage state, and E denotes exposed assets in low-lying zones. The components of $B(t)$ are formalized in Eq. (13).

This paper therefore treats the conventional return period as an input descriptor, not as the final safety metric. We retain return-period scenarios because they are embedded in Chinese flood-control practice and in the available project data. We then translate them into boundary-specific water levels, threshold exceedance, inundation-area response, and effective protection capacity. The proposed management shift is from 'what return period is the flood?' to 'which boundary combination causes which threshold to be exceeded, and which intervention breaks that pathway?' The evidence-led boundary-vector workflow connecting these elements is summarized in Fig. 1.

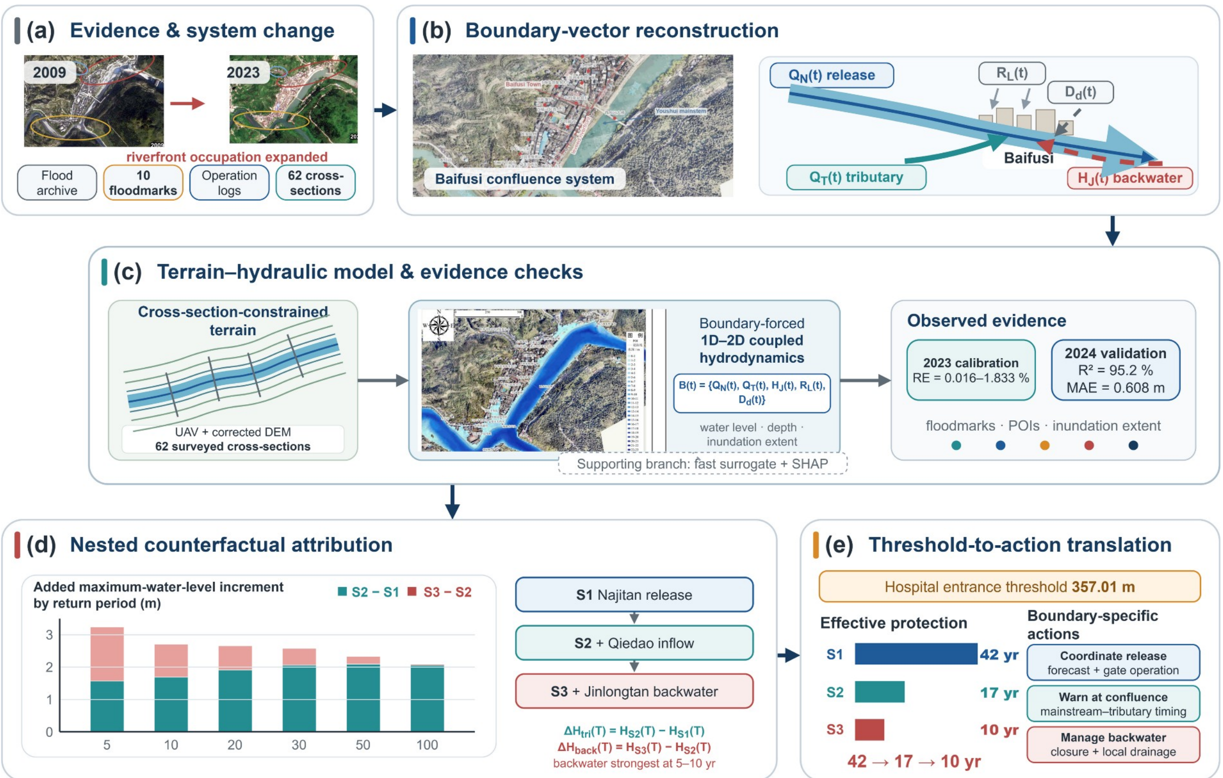

Figure 1. Evidence-led boundary-vector workflow for diagnosing compound flood-risk transformation in Baifusi. (a) Historical imagery and multi-source records document riverfront expansion and system change. (b) The reconstructed boundary vector comprises Najitan release Q_N(t), Qiedao tributary inflow Q_T(t), Jinlongtan downstream stage/backwater H_J(t), local rainfall–runoff R_L(t), and drainage state D_d(t). (c) Surveyed cross-sections constrain the river geometry used with the one-dimensional–two-dimensional coupled hydrodynamic model; the 2023 event provides project validation, while independent-event and surrogate evidence provide complementary checks (Xiao et al., 2026). (d) Matched nested scenarios —S1, Najitan/mainstream forcing with Qiedao inflow excluded and a non-backwater downstream condition; S2, S1 plus Qiedao design inflow under the same downstream condition; and S3, S2 with Jinlongtan backwater imposed—separate the tributary contribution ΔH_{tri}(T) = H_{S2}(T) − H_{S1}(T) and backwater contribution ΔH_{back}(T) = H_{S3}(T) − H_{S2}(T). (e) Linear interpolation against the 357.01 m hospital-entrance threshold translates these differences into approximate effective protection capacities of 42, 17, and 10 years under S1, S2, and S3, respectively, and identifies boundary-specific management actions. RE, relative error; R^2, coefficient of determination; MAE, mean absolute error; UAV, unmanned aerial vehicle; DEM, digital elevation model; POI, point of interest. All panels were drawn or redrawn from the authors' original project survey, monitoring, model, and GIS data. Geographical base data were supplied by the competent natural-resources authority of Hubei Province and are used under authorization for the government project.

https://doi.org/10.5194/egusphere-2026-4327
Preprint. Discussion started: 17 August 2026

2 Study area and evidence base

Baifusi is located in a mountainous reach of the Youshui River system. The town occupies a narrow valley environment where riverfront streets, bridges, low-lying land, and steep mountain runoff pathways interact over short distances. The settlement has historical and cultural importance, which makes flood management a heritage-protection issue as well as an engineering problem. The river corridor is also heavily engineered. Najitan Reservoir affects upstream flood release, Jinlongtan Reservoir affects downstream water levels and backwater conditions, and levee and riverfront works shape the local exchange between river flooding and internal drainage.

Local background records clarify the physical setting. Baifusi Town lies at the southern end of Laifeng County near the Hubei-Hunan-Chongqing border and covers about 190.14 km^2. The Youshui River runs north-south through the town, while the Qiedao River, a first-order tributary of the Youshui, runs west-east and joins the mainstream at the town. The Qiedao River has a county-reach length of about 30 km, a bed slope of approximately 1.8×10^{-3}, a channel width of about 20-100 m, and a catchment area of about 220 km^2. These values strengthen the interpretation that Baifusi is not a simple single-channel floodplain but a short-response confluence town where tributary inflow can rapidly change local thresholds.

The evidence base includes a Baifusi flood-safety project report, team-owned hydrodynamic and reservoir-operation datasets, historical image interpretation, floodmark records, drainage calculation materials and field photographs (Baifusi Project Team, 2024), summarized in Table 1 and Fig. 2. These sources provide complementary evidence. The project report supplies event records, observed flood levels, local thresholds, engineering background and policy recommendations. The reservoir-operation dataset provides data on Najitan operation, feature selection and rule extraction. Terrain-fusion and hydrodynamic modelling records provide cross-section correction, model calibration, validation and surrogate-model interpretation.

The monitoring network provides station-level support. The local network includes the Anfusi water-level station on the Qiedao River, rain gauges at Jingzhu and Maodong, the Baifusi water-level/rainfall station, and reservoir stations at Najitan and Jinlongtan. These stations make it possible to diagnose the 2023 flood as a time-dependent coupling of upstream release, tributary flow, downstream backwater and local rainfall.

Table 1. Evidence base and analytical role in the compound-flood diagnosis.

Evidence block	Variables or coverage	Analytical role
Historical flood and floodmark record	1963–2024 event accounts; 10 surveyed floodmarks; threshold water levels	Event-rate shift, flood-level timeline and threshold interpretation
Field survey and cross-sections	3.6 km^2 terrain area; 11 km mainstem; 2.4 km Qiedao reach; 62 sections	Model geometry, terrain correction and hydraulic validation

https://doi.org/10.5194/egusphere-2026-4327
Preprint. Discussion started: 17 August 2026

Evidence block	Variables or coverage	Analytical role
Hydrometeorological and reservoir monitoring	Rain gauges, water-level stations and Najitan/Jinlongtan operation records	Typical-event comparison and time-varying boundary construction
Engineering and governance records	Najitan 2007; Jinlongtan 2009; 10-year levee/road standard; 344.5 m Jinlongtan normal pool	Engineering chronology and boundary-control diagnosis
Remote-sensing and exposure evidence	2009 and 2023 images of low-lying riverfront and confluence areas	Qualitative exposure-migration evidence; no unsupported building-area quantification
Hydrodynamic and surrogate outputs	Mainstream-only, tributary-added and backwater-added scenario outputs; 37 design floods; 96 scenario samples; Shapley additive explanations (SHAP) checks	Boundary attribution, protection-capacity estimate and fast risk screening

https://doi.org/10.5194/egusphere-2026-4327
Preprint. Discussion started: 17 August 2026

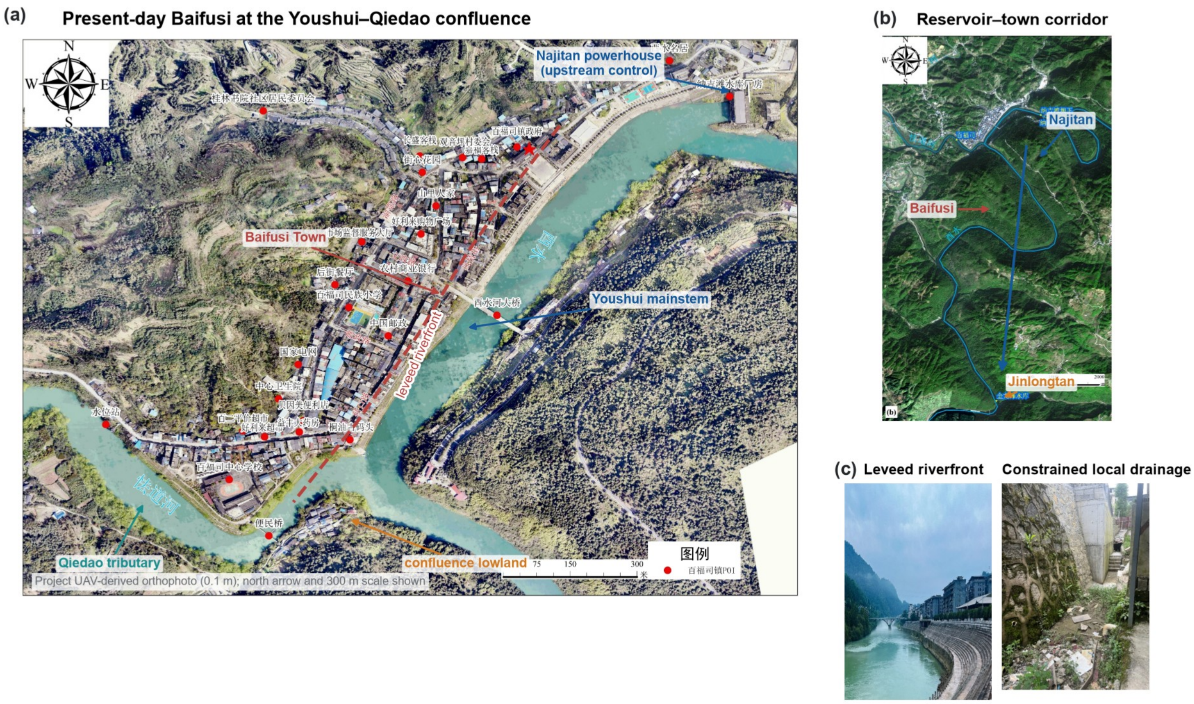

Figure 2. Present-day spatial configuration of the Baifusi compound-flood system. (a) Project UAV-derived digital orthophoto (0.1 m spatial resolution) showing Baifusi at the Youshui–Qiedao confluence, the upstream Najitan powerhouse, the leveed riverfront and the confluence lowland; a north arrow and 300 m scale are embedded in the source map. (b) Author-prepared research-site satellite map locating Najitan, Baifusi and Jinlongtan along the engineered river reach. (c) Field-survey photographs of the leveed riverfront and a constrained local drainage path. All panels were prepared from the authorized project UAV orthophoto, satellite base map, the authors' original project GIS/survey materials, and field photographs taken by the authors. Geographical base data were supplied by the competent natural-resources authority of Hubei Province and are used under authorization for the government project.

The flood-record evidence indicates a marked frequency change. During the 1963-2007 reference period, two serious flood-disaster events were recorded over 45 years, corresponding to about 0.044 events per year. In the recent 20-year record, eight town-inundation events were reported, corresponding to 0.400 events per year. The recent 10-year project-report count gives four events in 10 years, also 0.400 events per year. The resulting rate ratio is about 9 relative to the reference period. Because event counts are small, the statistical confidence interval is necessarily wide, and the result should be interpreted as an order-of-magnitude increase rather than a precisely estimated multiplicative factor. Still, the direction and practical importance of the change are clear.

The expanded historical-flood document shows that Laifeng County and Baifusi have long experienced destructive mountain floods. This does not weaken the paper's argument. Instead, it clarifies the research question: the issue is

https://doi.org/10.5194/egusphere-2026-4327
Preprint. Discussion started: 17 August 2026

not whether floods existed historically, but why a town with long-term adaptation has recently experienced repeated street-entry and town-inundation thresholds. The historical archive also shows that county-scale disasters and town-inundation thresholds must be distinguished carefully.

The most important recent events include 2016, 2021, 2023, and 2024. The 2016 flood had a reported highest flood level of 358.50 m, with house inundation up to 2.53 m. The 2021 and 2023 events produced street-entry and town inundation under rainstorm and tributary-confluence conditions. The 2024 event is especially useful as a contrast: Baifusi received only 22 mm of 1 d rainfall and Qiedao tributary inflow was relatively small, but the mainstream flood still produced high water levels. The combination of these events suggests multiple pathways to risk: local rainfall, tributary inflow, mainstream external flood, regulated release, and downstream boundary effects.

Local threshold data are central to the analysis. The emergency plan gives a super-standard flood reference level of 355.15 m. Reported street-entry thresholds are about 356.01 m at the old gas station, 357.01 m at the hospital entrance, and 357.30 m at Gutongyou wharf. These points convert a hydraulic water level into practical impact. If a scenario exceeds these thresholds, the event is no longer an abstract return-period flood but a flood that enters the town's functional spaces.

The evidence base was graded according to how directly it supports each claim. Strong evidence was assigned to claims backed by event data, hydraulic scenarios, threshold exceedance, and model-validation metrics. Medium evidence was assigned to mechanisms supported by project-report interpretation and visual or descriptive material but not yet by a complete quantitative time series, such as levee-drainage side effects and exposure expansion. This grading affects the language used in the manuscript. For example, the tributary and backwater effects are treated as quantified results, whereas the exposure-expansion pathway is treated as a locally supported and plausible amplification mechanism that should be strengthened with historical land-use maps and building-footprint data before being framed as a fully quantified causal effect.

This distinction is important for avoiding overclaiming. The paper's central hydraulic conclusions are supported by nested scenarios, validation records, and threshold comparison. The broader human-water interpretation is supported by convergence between the hydraulic results, project-report statements, observed riverfront development, and known mechanisms of residual risk accumulation behind protection. The manuscript therefore uses different levels of certainty: 'shows' or 'indicates' for quantified hydraulic findings, 'suggests' for synthesized risk-system interpretations, and 'may' or 'is consistent with' for mechanisms that require additional spatial data.

https://doi.org/10.5194/egusphere-2026-4327
Preprint. Discussion started: 17 August 2026

3 Data and methods

3.1 Analytical framework

The evidence-to-action workflow used in this study is summarized in Fig. 1. Multi-source observations first document system change and reconstruct the five-component boundary vector. Fused terrain and the time-varying boundaries then drive the one-dimensional–two-dimensional coupled hydrodynamic model, whose credibility is assessed using 2023 calibration and independent 2024 validation. Matched nested scenarios S1–S3 isolate the water-level contributions of Qiedao tributary inflow and Jinlongtan backwater. Finally, comparison with the 357.01 m hospital-entrance threshold converts these contributions into effective protection-capacity estimates and boundary-specific actions. The surrogate-model and SHAP results provide supporting interpretability evidence rather than the primary causal attribution.

Event frequency was summarized by the event rate and the rate ratio in Eq. (2). Here N_i is the number of reported inundation events in period i and L_i is the period length in years. These metrics are used only as descriptive indicators because the event count is small.

$$\lambda_i = \frac{N_i}{L_i}, \qquad RR = \frac{\lambda_{recent}}{\lambda_{reference}} \tag{2}$$

For a reservoir flood-regulation event, peak-reduction efficiency was calculated with Eq. (3), where $Q_{in,p}$ is the inflow peak and $Q_{out,p}$ is the release peak.

$$\eta = [(Q_{in,p} - Q_{out,p}) / Q_{in,p}] \times 100\ \% \tag{3}$$

For the 2023 event, $Q_{in,p} = 4727.11\ \mathrm{m^3\ s^{-1}}$ and $Q_{out,p} = 4000\ \mathrm{m^3\ s^{-1}}$, giving η = 15.38 %.

For each return period T, the marginal water-level effects of tributary inflow, downstream backwater, and their compound action were calculated with Eq. (4).

$$\begin{aligned} \Delta H_{tri}(T) &= H_{S2}(T) - H_{S1}(T), \\ \Delta H_{back}(T) &= H_{S3}(T) - H_{S2}(T), \\ \Delta H_{comp}(T) &= H_{S3}(T) - H_{S1}(T) \end{aligned} \tag{4}$$

The corresponding inundation-area responses were calculated with Eq. (5).

https://doi.org/10.5194/egusphere-2026-4327
Preprint. Discussion started: 17 August 2026

$$r_{tri}(T) = \frac{[A_{S2}(T) - A_{S1}(T)]}{A_{S1}(T)} \times 100\ \%,$$
$$r_{back}(T) = \frac{[A_{S3}(T) - A_{S2}(T)]}{A_{S2}(T)} \times 100\ \% \tag{5}$$

Threshold exceedance was calculated with Eq. (6), where H_k is a local threshold such as the emergency-plan level or a street-entry level. Positive E_k indicates that the hydraulic scenario exceeds the impact threshold. Threshold-specific crossings are used for diagnosis; the effective protection capacities reported in this manuscript use the hospital entrance threshold (357.01 m) and are obtained by return-period interpolation within each scenario family.

$$E_k(S,\ T) = H_S(T) - H_k \tag{6}$$

The analysis follows a multi-boundary attribution design. Instead of treating the river discharge, tributary input, and downstream water level as a single combined forcing, the framework separates them into nested counterfactual scenarios (Table 2). S1 represents the mainstream or Najitan-release boundary alone. S2 adds Qiedao tributary inflow and therefore isolates the tributary-confluence effect as S2-S1. S3 adds Jinlongtan downstream backwater and therefore isolates the downstream-boundary effect as S3-S2. The total compound effect is S3-S1.

This design is not a fully randomized causal experiment, but it is a strong physical counterfactual within the limits of hydrodynamic modelling. It tests whether the town's flood level and inundation area change when specific hydraulic boundaries are included, while keeping the scenario structure transparent. The same framework is then linked to local thresholds and protection-capacity estimates.

Boundary synchronization assumption. For design-scenario comparison, S1, S2 and S3 are interpreted as nested counterfactuals for the same return-period class. The comparison therefore isolates the marginal effect of adding Qiedao inflow and Jinlongtan backwater under otherwise matched mainstream forcing. For event diagnosis, the observed timing is used where available: the 2023 event combined a Najitan inflow peak of 4727.11 $m^3\ s^{-1}$, a maximum release of 4000 $m^3\ s^{-1}$ sustained for about 7 h, a Qiedao tributary peak of 1240 $m^3\ s^{-1}$, and a Jinlongtan upstream water level of 351.02 m. These observed values support the interpretation that damaging floods arise from boundary co-occurrence rather than from rainfall magnitude alone.

The framework deliberately separates hazard generation, hydraulic amplification, and impact conversion. Hazard generation includes mainstream flood inflow, tributary runoff, and reservoir release. Hydraulic amplification includes confluence stage rise and downstream backwater. Impact conversion occurs when water levels exceed local thresholds at streets, public facilities, or riverfront buildings. This separation prevents the common analytical shortcut

https://doi.org/10.5194/egusphere-2026-4327
Preprint. Discussion started: 17 August 2026

of treating rainfall, discharge, water level, and damage as one undifferentiated flood variable. It also makes the analysis useful for management because different parts of the chain require different interventions.

Table 2. Boundary-vector scenarios and model-design conditions. ΔH_{tri} and ΔH_{back} denote the tributary- and backwater-induced water-level increments, respectively.

Scenario	Upstream boundary	Tributary boundary	Downstream boundary	Diagnostic purpose	Outputs
S1	Najitan/mainstream release	Excluded	Free/maximum downstream release condition	Mainstream-only reference boundary	Peak level, inundation area
S2	Same as S1	Qiedao design inflow added	Same as S1	Marginal tributary contribution	ΔH_{tri}, area increment
S3	Same as S2	Same as S2	Jinlongtan backwater imposed	Compound boundary with downstream tailwater	ΔH_{back}, effective capacity
2023 replay	Observed Najitan release and reservoir level	Observed/ estimated tributary contribution	Observed Jinlongtan tailwater	Historical event validation	Floodmarks, water level, inundation pattern
Optimized routing test	Pre-release and reduced safe release target	Same 2023 storm setting	Operational constraint retained	Assess whether operation window can reduce compound pressure	Peak reduction, release, pool level

3.2 Event-frequency and typical-event comparison

Flood-inundation frequency was evaluated using reported event counts. Event rate was computed as the number of events divided by the duration of the period. The reference period was 1963-2007. The recent periods were the most recent 20 years and 10 years reported in the project material. Because the counts are small, the analysis uses cautious language and treats the rate ratio as an indicator of practical change rather than a definitive trend test.

Typical events in 2021, 2023, and 2024 were compared using Najitan inflow peak, Najitan release, downstream water level below Najitan, Jinlongtan upstream water level, Qiedao tributary peak, Baifusi 1 d rainfall, and Laifeng hydrological-station peak. The purpose was to distinguish event types: rainstorm-confluence events, backwater-amplified compound events, and mainstream external-flood events.

The 2023 monitoring records allow the 25 July event to be described with hourly evidence. In the integrated monitoring table for 21-31 July 2023, Najitan reservoir level reached 369.96 m at 18:00 on 25 July, Najitan dam-downstream water level reached 358.20 m at the same time, Jinlongtan reservoir level reached 351.07 m at 20:00, and

https://doi.org/10.5194/egusphere-2026-4327
Preprint. Discussion started: 17 August 2026

the Anfusi station on the Qiedao River reached 360.11 m and 1240 $m^3 s^{-1}$ at 17:00. The Baifusi town station reached 354.949 m at 19:00. These timings show that tributary, upstream and downstream boundaries peaked within a few hours, which is exactly the compound-boundary condition tested by the scenario framework.

The stand-alone Najitan CSV for 23-26 July records a maximum release of 4000 $m^3 s^{-1}$ at 15:00 on 25 July, whereas the integrated monitoring workbook records 4700 $m^3 s^{-1}$ at 18:00 on the same day. Because these sources are not yet reconciled, the event is treated as a high-release process of 4000-4700 $m^3 s^{-1}$, and analyses requiring the exact operational boundary should be interpreted as provisional.

The event comparison is used as a diagnostic matrix rather than as a statistical classifier. With only three detailed recent events, a supervised classification model would be inappropriate. A transparent matrix is more defensible: it shows which boundary was large, which boundary was small, and whether inundation or high warning levels occurred. This choice follows the principle that the complexity of an analytical tool should match the amount and quality of evidence available.

The meteorological-hydrological diagnosis was organized as a boundary-state reconstruction rather than as a rainfall-only frequency analysis. Rainfall, reservoir inflow, reservoir release, tributary flow and downstream stage were first converted to a common event timeline. Event severity was then described by 24 h rainfall return period, mainstream inflow peak, controlled release peak, tributary peak, peak timing difference and downstream water level. This procedure is necessary in a reservoir-affected mountain reach because the same rainfall amount can produce different town water levels depending on antecedent reservoir storage, gate operation, tributary synchronization and tailwater stage.

Design flood boundaries were therefore treated as process hydrographs. Where natural-flow information was needed, reservoir routing was interpreted through the water-balance relation in Eq. (7), where V is reservoir storage, Q_{in} is inflow, and Q_{out} is release. In practical terms, measured release and stage-storage curves allow inflow reconstruction by a tabular trial or finite-difference routing method, while observed reservoir releases provide the regulated boundary imposed on the downstream town reach. This distinction between natural inflow and operational release is central to the paper's argument: flood risk cannot be inferred from a single nominal return period after regulation has altered both the magnitude and timing of the flood wave.

$$\frac{dV}{dt} = Q_{\mathrm{in}}(t) - Q_{out}(t) \tag{7}$$

3.3 Reservoir-operation representation

Najitan operation was represented as a dynamic upstream boundary rather than a fixed design-flow assumption. The reservoir has a normal pool level of 370.00 m, a dead water level of 366.50 m, maximum release capacity of 9230 $m^3 s^{-1}$, and regulation storage of 9.71 million m^3. Operation data from 2013-01 to 2023-12 were used for training, and data from 2024-01 to 2024-10 were used for testing in the reservoir-operation dataset.

Decision tree, random forest, and LightGBM models were compared under F-test and mutual-information feature-selection routes. The F-test LightGBM model had the best overall performance among the reported models (R^2 = 0.9631, MAE = 11.7997, RMSE = 40.9632 $m^3 s^{-1}$, MAPE = 15.5019). In this manuscript the model is used as a dispatch-rule extractor: it shows that reservoir release can be learned from hydrometeorological and operational predictors and therefore should be treated as a dynamic engineering boundary in flood-risk analysis.

The operation-rule learning problem was formulated as a supervised regression task in which the target variable is hourly reservoir release and the predictors describe the hydrological and operational state of the reservoir system. Candidate predictors include inflow-related variables, reservoir water level, antecedent release, storage-state indicators and time-lagged process variables. The F-test route ranks variables according to their linear explanatory power for release, whereas the mutual-information route captures nonlinear dependence. The two filters were used to test whether the learned rule was robust to different assumptions about the relation between state variables and release decisions.

Model learning followed a three-step sequence. First, each feature-selection route generated a candidate state vector. Second, decision tree, random forest and LightGBM regressors were trained to approximate the observed mapping from state vector to release. Third, hyperparameters, including the candidate-feature number and tree-complexity controls, were optimized with a tree-structured Parzen-estimator Bayesian search. The six resulting models, FR-DT, MIR-DT, FR-RF, MIR-RF, FR-LGB and MIR-LGB, were evaluated with R^2, mean absolute error (MAE), root mean square error (RMSE) and mean absolute percentage error (MAPE) on the 2024 test period.

The reservoir-operation model is not used here to replace official gate-operation rules. Its role is more limited and more defensible: it extracts the empirical release response embedded in long-term monitoring records and provides a dynamic upstream boundary for hydraulic diagnosis. The high test performance of FR-LGB implies that the operational boundary is learnable from observed state variables, so treating Najitan release as a fixed design hydrograph would discard information about human control of the flood wave.

https://doi.org/10.5194/egusphere-2026-4327
Preprint. Discussion started: 17 August 2026

3.4 Terrain reconstruction, coupled hydrodynamic simulation, and surrogate modelling

The one-dimensional channel geometry was reconstructed from 62 surveyed cross-sections: 47 along the Youshui mainstream between Najitan and Jinlongtan and 15 along the Qiedao tributary. The sections were spaced at about 200–300 m and covered approximately 11 km of mainstream channel and 2.4 km of tributary channel. Field elevation points were used to construct the locally refined two-dimensional town floodplain. A related terrain-fusion analysis showed that correcting submerged channel elevations materially affects simulated inundation (Xiao et al., 2026); its 10 m fused-DEM metrics are shown in Fig. 3 as supporting evidence and are not the computational grid used for the S1–S3 HydroMPM scenarios.

The hydraulic model couples a one-dimensional river-channel component, governed by the Saint-Venant continuity and momentum equations, to a two-dimensional floodplain component governed by the depth-averaged shallow-water equations. Lateral exchange between the channel and floodplain is represented with a broad-crested-weir relation. Eqs. (8)-(10) summarize the two-dimensional component.

$$\frac{\partial h}{\partial t} + \frac{\partial (hu)}{\partial x} + \frac{\partial (hv)}{\partial y} = q, \tag{8}$$

$$\frac{\partial (hu)}{\partial t} + \frac{\partial \left(hu^2 + \frac{gh^2}{2}\right)}{\partial x} + \frac{\partial (huv)}{\partial y} = gh(S_{0,x} - S_{f,x}), \tag{9}$$

$$\frac{\partial (hv)}{\partial t} + \frac{\partial (huv)}{\partial x} + \frac{\partial \left(hv^2 + \frac{gh^2}{2}\right)}{\partial y} = gh(S_{0,y} - S_{f,y}). \tag{10}$$

Here h is water depth, u and v are depth-averaged velocities, q denotes lateral source or sink terms, g is gravitational acceleration, S0 is bed slope, and Sf is the roughness-dependent friction slope. The equations are provided to identify the hydraulic controls rather than as a new solver contribution.

The modelling workflow was to (i) construct the one-dimensional Youshui–Qiedao river network from the surveyed centreline and cross-sections; (ii) generate and roughness-parameterize the two-dimensional town floodplain mesh; (iii) connect the two domains through lateral coupling lines; (iv) impose Najitan release, Qiedao inflow, and Jinlongtan stage or rating boundaries for each scenario; (v) check the coupled model against the surveyed 2023 flood; and (vi) extract maximum water level, maximum depth, inundation area, and threshold exceedance.

The S1–S3 scenarios were simulated with HydroMPM FloodRisk as a one-dimensional–two-dimensional coupled model. Its two-dimensional solver is based on the robust well-balanced Godunov-type finite-volume model proposed by Song et al. (2011) for wetting and drying over irregular terrain. The one-dimensional domain extends from the

https://doi.org/10.5194/egusphere-2026-4327
Preprint. Discussion started: 17 August 2026

Najitan dam downstream along the Youshui mainstream, includes the Qiedao tributary, and terminates at the Jinlongtan reservoir boundary. The two-dimensional domain covers 5.75 km² of the town floodplain and contains 22,787 locally refined unstructured triangular cells; 50 lateral coupling lines connect the left and right banks to the floodplain mesh. Najitan release and Qiedao inflow are discharge boundaries, whereas Jinlongtan is represented by a stage or stage–discharge boundary.

Validation of the coupled model emphasized the observed inundation pattern and floodmark depths during the 25 July 2023 event. The field survey recorded widespread inundation at the Youshui–Qiedao confluence and overflow along the upstream mainstream. The coupled model was evaluated against these locations and the measured floodmark depths before the nested scenario differences were interpreted.

The model configuration table distinguishes quantities fixed in the analysis from boundary files that are not currently available for independent reproduction. This distinction matters because the paper's principal claim depends on scenario differences, not on a single absolute design water level.

For the 25 July 2023 event, the coupled model reproduced the extensive inundation at the Youshui–Qiedao confluence and the upstream-mainstream overflow zone. The simulated maximum water level at the confluence was 358.03 m, about 1.03 m above the local 357 m levee crest, and differences between surveyed floodmarks and simulated depths were within 0.1 m. Fig. 3 summarizes this project validation together with complementary terrain, independent-event, reservoir-operation, and surrogate-model evidence.

The terrain-fusion and forecasting study also developed an interpretable surrogate model (Xiao et al., 2026). Thirty-seven design-flood scenarios and four independent test groups were used. The published surrogate retained eight explanatory variables: elevation, Najitan/mainstream peak discharge, plan curvature, Najitan/mainstream time to peak, roughness, Najitan/mainstream average discharge up to the peak, Anfusi/Qiedao tributary peak discharge, and Najitan/mainstream flood duration. The surrogate achieved average POD = 95.977 %, FAR = 3.109 %, and average test R^2 = 98.6 % for maximum water depth. These previously published results are cited here only as supporting evidence for the reliability of the urban hydrodynamic and interpretability framework. The engineering attribution in the present study is instead based on the boundary vector and matched scenarios defined in Sect. 3.1 and Table 2.

The interpretability step used Shapley additive explanations (SHAP). The feature contribution and its weight were expressed in Eqs. (11)-(12).

$$\varphi_j = \sum_{S \subseteq F \setminus \{j\}} w(S)[f(S \cup \{j\}) - f(S)] \quad (11)$$

$$w(S) = \frac{|S|!\,(|F| - |S| - 1)!}{|F|!}. \quad (12)$$

https://doi.org/10.5194/egusphere-2026-4327
Preprint. Discussion started: 17 August 2026

Here F is the full feature set, S is a feature subset and f(·) is the model prediction. The sign and magnitude of φ_j indicate whether a feature increases or decreases predicted water depth for a given sample. In this paper, SHAP evidence is used as supporting physical interpretation: low elevation and low plan curvature identify internal terrain susceptibility, whereas mainstream peak and tributary peak identify external hydraulic pressure.

This surrogate component strengthens, but does not replace, the hydrodynamic scenario evidence. Its main value for the present manuscript is explanatory triangulation. If the hydrodynamic scenarios show that Qiedao inflow and Jinlongtan backwater lower the effective protection capacity, and the SHAP results independently identify flood peaks, elevation, roughness and curvature as physically meaningful drivers, then the threshold-migration interpretation is supported by both process simulation and interpretable data-driven approximation.

https://doi.org/10.5194/egusphere-2026-4327
Preprint. Discussion started: 17 August 2026

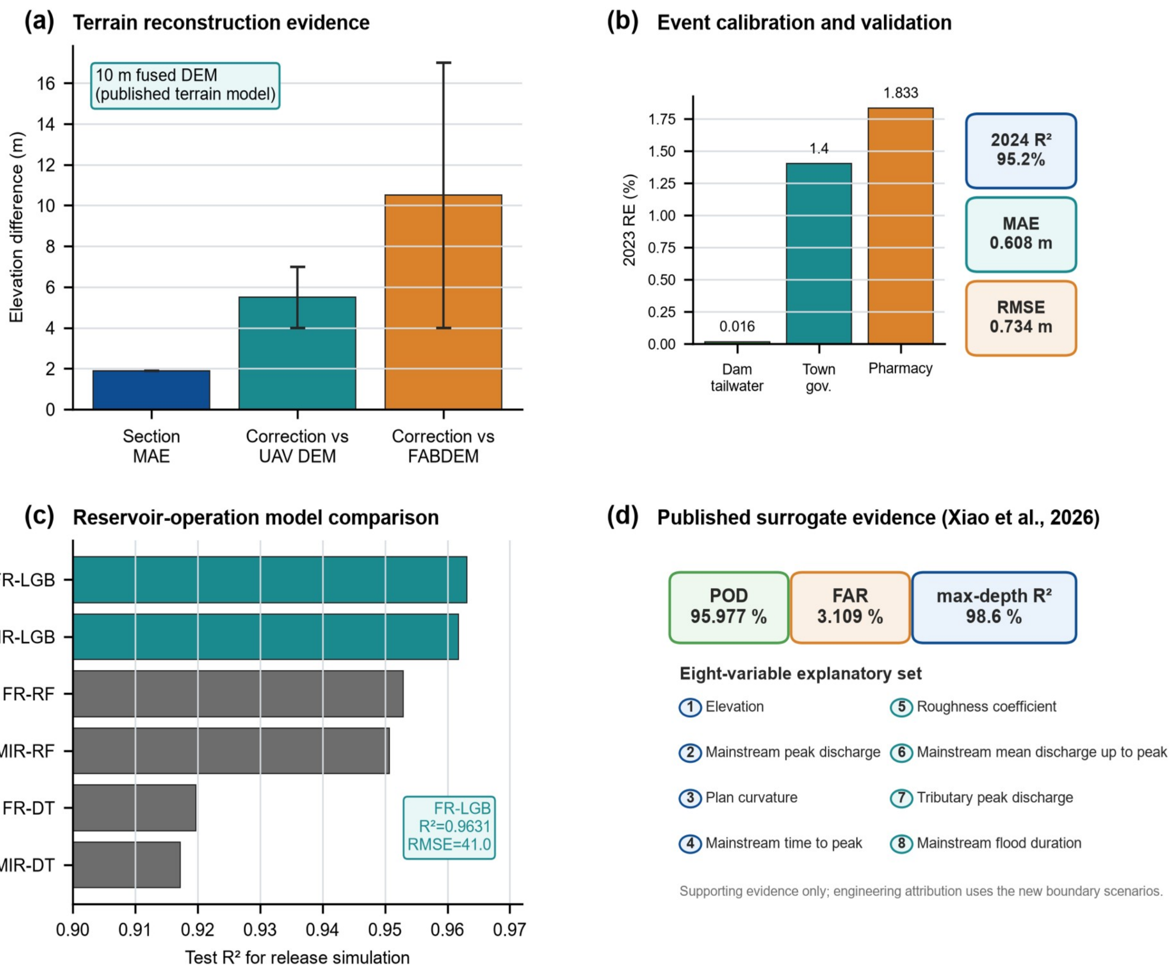

Figure 3. Model reliability and fast-simulation evidence. (a) Terrain reconstruction and DEM correction evidence. (b) 2023 event calibration errors and 2024 independent validation metrics. (c) Reservoir-operation model comparison showing the selected LightGBM representation. (d) Previously published surrogate-model performance and its eight-variable explanatory set. Panels (a), (b), and (d) summarize previously published terrain, validation, and surrogate evidence from Xiao et al. (2026); panel (c) reports the reservoir-operation comparison used in the present study. All panels were newly redrawn from the authors' original project and model data; no published graphical artwork was reproduced.

3.4.1 Detailed hydrodynamic workflow and boundary-vector diagnosis

The present analysis treats the hydraulic model as a process-diagnostic system rather than as a single design-flood mapping exercise. The computational boundary vector is defined in Eq. (13).

https://doi.org/10.5194/egusphere-2026-4327
Preprint. Discussion started: 17 August 2026

$$B(t) = \{Q_N(t),\ Q_T(t),\ H_J(t),\ R_L(t),\ D_d(t)\} \tag{13}$$

Here Q_N(t) is the Najitan release hydrograph at the model's upstream boundary (or the matched mainstream design hydrograph in design scenarios), Q_T(t) is the Qiedao tributary inflow, and H_J(t) is the Jinlongtan downstream-stage boundary. R_L(t) and D_d(t) describe local rainfall–runoff and drainage state in the broader diagnostic framework; they are not varied in the S1–S3 boundary-attribution experiments.

Terrain preprocessing followed four steps: (i) fusion of UAV survey, field topographic points and river cross-sections; (ii) removal of bridge, building and levee artefacts that would block floodplain connectivity incorrectly; (iii) assignment of roughness zones for the main channel, vegetated bars, roads, dense residential blocks and hillside margins; and (iv) vertical-datum checking against floodmark elevations and monitored stages. The 2023 floodmark elevation of 358.22 m and the monitored peak stage of 358.20 m were used as a hard consistency check before scenario interpretation.

The model comparison uses nested scenario differences. For a diagnostic point or inundation metric M, the boundary-attribution increment is defined in Eq. (14), where M_i is the scenario result and M_{ref} is the preceding nested scenario.

$$\Delta M_i = max_t\ M_i(t) - max_t\ M_{ref}(t) \tag{14}$$

For exposure, the low-lying built-exposure ratio is expressed with Eq. (15), where I is the simulated inundation indicator and B_{low} is the interpreted low-lying built-up zone. In the present analysis this exposure ratio is treated qualitatively because the 2009–2023 building-footprint vectors are not yet available.

$$E_b = \frac{A(I > 0 \wedge B_{low} = 1)}{A(B_{low} = 1)} \tag{15}$$

Observed reservoir operation was introduced at the downstream boundary in two ways. First, Jinlongtan rule thresholds (1500 and 3200 $m^3\ s^{-1}$ and the 344.50 m control level) were used to define operational state transitions. Second, the July 2023 operation log was digitized to reconstruct gate-opening timing, spillway release and reservoir level. This avoids assuming that the downstream boundary is either a fixed rating curve or a constant normal pool.

3.5 Threshold and effective-capacity analysis

Scenario water levels were compared with local threshold levels. A water level exceeding 355.15 m indicates exceedance of the emergency-plan super-standard reference. Exceedance of 356.01, 357.01, and 357.30 m corresponds to street-entry thresholds at the old gas station, hospital entrance, and Gutongyou wharf, respectively. These comparisons translate modelled hydraulic states into impact-relevant conditions.

https://doi.org/10.5194/egusphere-2026-4327
Preprint. Discussion started: 17 August 2026

The threshold analysis treats flood risk as a transition from hydraulic load to social impact. Four threshold levels are used: the emergency-plan reference level, the old-gas-station street-entry level, the hospital-entrance public-service threshold and the Gutongyou-wharf riverfront threshold. These levels are not statistically fitted damage functions; they are observed or administratively meaningful switch points at which a hydraulic event changes into a management problem.

For each scenario, threshold crossing was evaluated as binary exceedance, exceedance margin, and return-period interpolation. Binary exceedance identifies whether $H_S(\mathrm{T}) > H_k$; the margin follows Eq. (6); and interpolation between adjacent return-period nodes estimates the effective capacity.

Effective protection capacity was estimated by identifying the return-period scenario at which the town-relevant thresholds are approached or exceeded under each boundary configuration. The scenario results indicate about 42-year capacity under the mainstream-only state, about 17-year capacity after adding Qiedao tributary inflow, and about 10-year capacity after adding Jinlongtan backwater. This capacity degradation is the main quantitative expression of risk transformation.

The capacity estimate is calculated with linear interpolation between adjacent return-period nodes. For scenario S and impact threshold H_k, if $H_S(\mathrm{T}_0) \le H_k \le H_S(\mathrm{T}_1)$, the effective protection capacity is estimated with Eq. (16).

$$C(S,\ H_k) = T_0 + \frac{H_k - H_S(T_0)}{H_S(T_1) - H_S(T_0)} \times (T_1 - T_0) \tag{16}$$

The manuscript uses the hospital entrance threshold, H_k = 357.01 m, as the controlling public-service threshold because it lies above minor street entry but below the higher wharf threshold. The rounded values reported in the Results are therefore threshold-specific estimates rather than universal design standards.

Threshold analysis was preferred over a damage-curve analysis because detailed building-level loss data were unavailable. This is a limitation, but it is also appropriate for the current decision problem. The town must know when water begins to enter key streets and public-service locations even before a complete monetary loss model is available. For heritage-town risk management, avoiding repeated entry into culturally and socially important spaces can be as important as estimating direct economic loss.

4 Results

4.1 Observed flood-risk escalation and event characteristics

The descriptive flood record indicates a marked change in damaging-inundation frequency. The reported rate increased from 0.044 events yr^{-1} in 1963–2007 to 0.400 events yr^{-1} in both the recent 20-year and recent 10-year project records, corresponding to a rate ratio of about 9 (Fig. 4a). Because the counts are small, this ratio is interpreted as a practical indicator rather than a formal stationary-trend estimate.

https://doi.org/10.5194/egusphere-2026-4327
Preprint. Discussion started: 17 August 2026

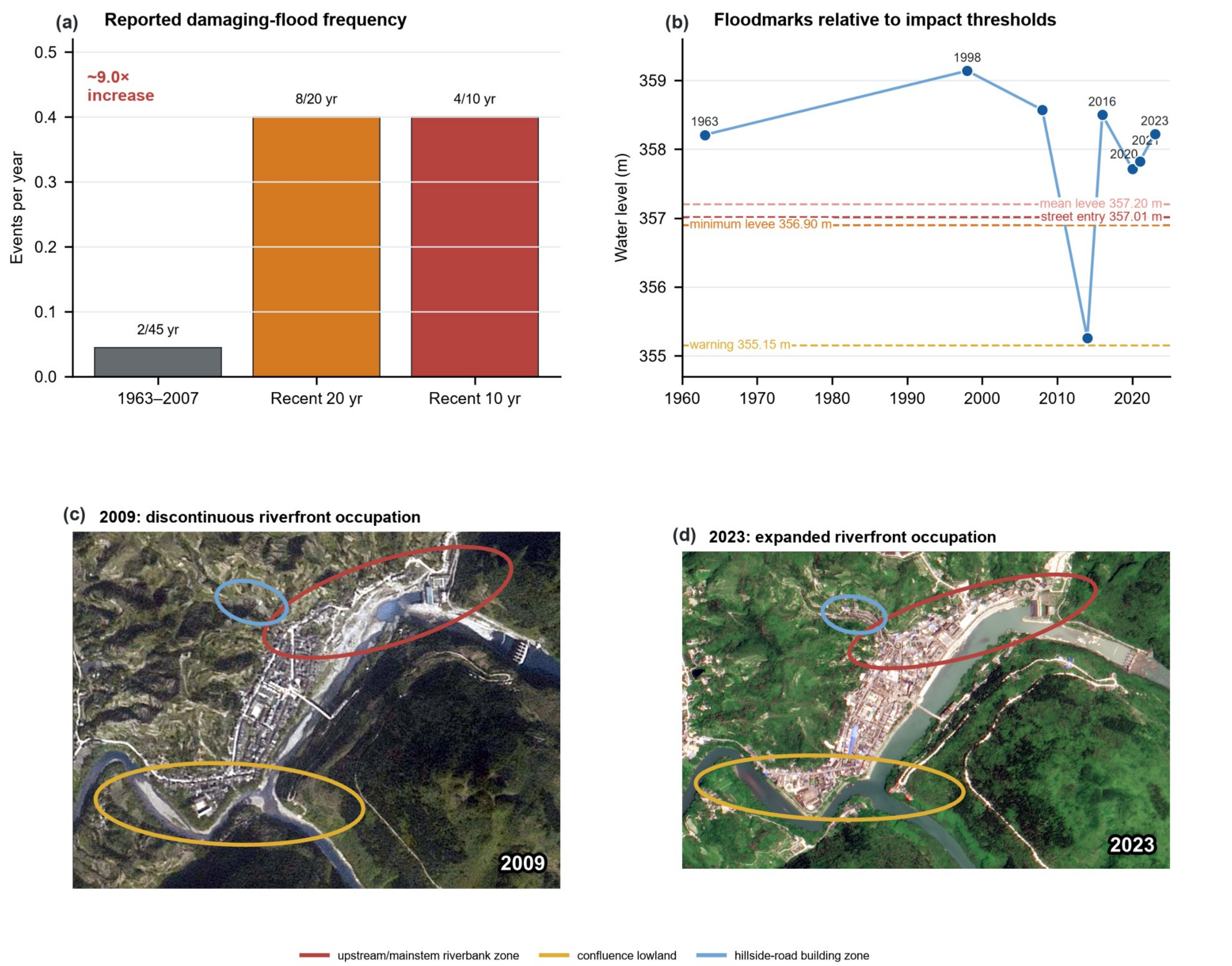

Figure 4. Historical flood-risk escalation and spatial exposure shift. (a) Reported damaging-inundation event rates for the reference and recent periods. (b) Floodmark water levels relative to operational and street-entry thresholds. (c, d) Project-archive spatial images for 2009 and 17 July 2023. Red, yellow and light-blue ellipses reproduce the comparison zones in the source material and denote the upstream/mainstem riverbank zone, confluence lowland and hillside-road building zone, respectively. The ellipses are qualitative comparison guides rather than mapped building-footprint polygons. The spatial panels were redrawn by the authors from original project GIS data and geographical base data supplied by the competent natural-resources authority of Hubei Province under authorization for the government project

The floodmark series shows that damaging water levels are not unique to the recent period, but recent events have repeatedly approached or exceeded locally meaningful warning, levee, and street-entry levels (Fig. 4b). The 2009 and 2023 spatial images also show denser occupation of the riverfront and confluence lowland in the later image (Fig.

https://doi.org/10.5194/egusphere-2026-4327
Preprint. Discussion started: 17 August 2026

4c,d). This image comparison is qualitative; the ellipses identify consistent comparison zones rather than quantified building-footprint change.

The 2021 and 2023 events combined large Najitan releases with substantial Qiedao inflow (Fig. 5 and Table 3). In 2021, Najitan inflow/release reached 4611.11/4000 $m^3\ s^{-1}$, Qiedao peaked at 1160 $m^3\ s^{-1}$, and Baifusi 24 h rainfall was 160.0 mm. In 2023, the corresponding values were 4727.11/4000 $m^3\ s^{-1}$, 1240 $m^3\ s^{-1}$, and 189.6 mm, while the Jinlongtan upstream water level reached 351.02 m.

For the 2023 event, the 24 h rainfall return period was about 7.75 years for the Youshui mainstream catchment, 3.26 years for Qiedao River, and 2.96 years for the Jinlongtan area (Fig. 5b–d). Najitan regulation reduced the reported inflow peak from 4727.11 to 4000 $m^3\ s^{-1}$, equivalent to 15.38 %; a separate routing scenario gave 18.5 % peak reduction. Damaging inundation therefore occurred despite moderate local rainfall return periods and measurable upstream peak attenuation.

The 2024 event had a different boundary signature. Local rainfall was 22 mm and the Qiedao peak was 260 $m^3\ s^{-1}$, whereas Najitan inflow reached 4116.11 $m^3\ s^{-1}$ and the Laifeng station peak reached 1971.6 $m^3\ s^{-1}$ (Table 3). The three-event comparison thus records both confluence-affected events and a high-mainstream event under weak local rainfall.

https://doi.org/10.5194/egusphere-2026-4327
Preprint. Discussion started: 17 August 2026

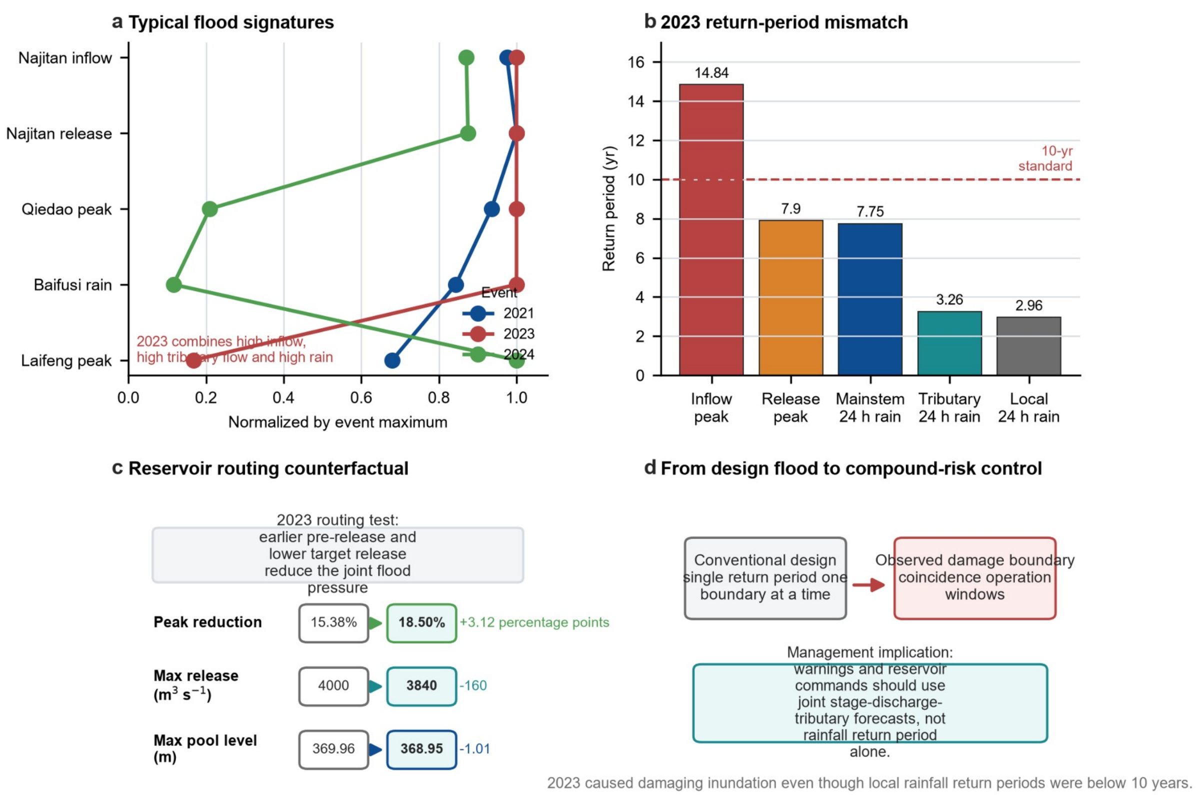

525 **Figure 5. Typical-event comparison and return-period mismatch. (a) Normalized signatures of the 2021, 2023 and 2024 events. (b) The 2023 event caused damaging inundation although local rainfall return periods were below the nominal 10-year standard. (c) Actual and optimized routing indicators. (d) Conceptual shift from single-driver return-period design to compound-risk control. All panels were newly drawn from the authors' original hydrometeorological, reservoir-operation, and project-analysis data**

530

https://doi.org/10.5194/egusphere-2026-4327
Preprint. Discussion started: 17 August 2026

Table 3. Typical flood-event signatures used for process attribution. Paired entries report Najitan inflow/release and Qiedao peak/local 24 h rainfall, respectively.

Event	Boundary state	Najitan inflow / release (m^3 s^{-1})	Qiedao peak / local 24 h rainfall (m^3 s^{-1} / mm)	Diagnostic meaning
2021	Rainstorm-confluence	4611.11 / 4000	1160 / 160.0	Release and Qiedao coincide
2023	Tributary/backwater	4727.11 / 4000	1240 / 189.6	Moderate rainfall with compound boundaries
2024	External-mainstream dominated	4116.11 / 3500	260 / 22.0	High mainstream pressure with weak local rainfall

4.2 Boundary-specific hydraulic contributions

Under matched return-period forcing, the S2−S1 difference isolates the effect of adding Qiedao tributary inflow (Fig. 6a,b; Table 4). The maximum-water-level increment was 1.56 m at 5 years, 1.68 m at 10 years, 1.90 m at 20 years, 2.05 m at 30 years, 2.08 m at 50 years, and 2.05 m at 100 years.

The S3−S2 difference isolates the Jinlongtan downstream-boundary contribution. The maximum-water-level increment was 1.67, 1.02, 0.75, 0.52, 0.24, and 0.03 m for the 5-, 10-, 20-, 30-, 50-, and 100-year scenarios, respectively (Fig. 6b).

The tributary increment therefore remained between 1.56 and 2.08 m across all six return periods, whereas the marginal backwater increment decreased from 1.67 m at 5 years to 0.03 m at 100 years. The total S3−S1 rise decreased from 3.23 m in the 5-year scenario to 2.08 m in the 100-year scenario (Table 4).

4.3 Inundation response and effective protection capacity

Interpolation against the 357.01 m hospital-entrance threshold gave an effective protection capacity of about 42 years under S1, 17 years under S2, and 10 years under S3 (Fig. 6d). Thus, the tributary-added and full compound boundaries shifted the threshold crossing into progressively more frequent return-period classes.

The absolute scenario levels show how this shift reaches local impact points. Under S3, the 5-year level was 355.96 m, above the 355.15 m emergency-plan reference. The 10-year level was 357.08 m, above both the 356.01 m old-gas-station threshold and the 357.01 m hospital-entrance threshold (Fig. 6a; Table 4).

Adding Qiedao inflow increased inundation area by 23.6 %, 22.6 %, 32.1 %, 53.3 %, 76.9 %, and 62.2 % for the 5-, 10-, 20-, 30-, 50-, and 100-year scenarios, respectively (Fig. 6c; Table 4). The tributary contribution was therefore present throughout the assessed range.

https://doi.org/10.5194/egusphere-2026-4327
Preprint. Discussion started: 17 August 2026

Adding Jinlongtan backwater increased inundation area by 24.3 %, 18.5 %, 19.0 %, and 20.5 % for the 5-, 10-, 20-, and 30-year scenarios, respectively, but by only 6.4 % and 0.6 % for the 50- and 100-year scenarios. The area response therefore followed the same return-period dependence as the water-level increment.

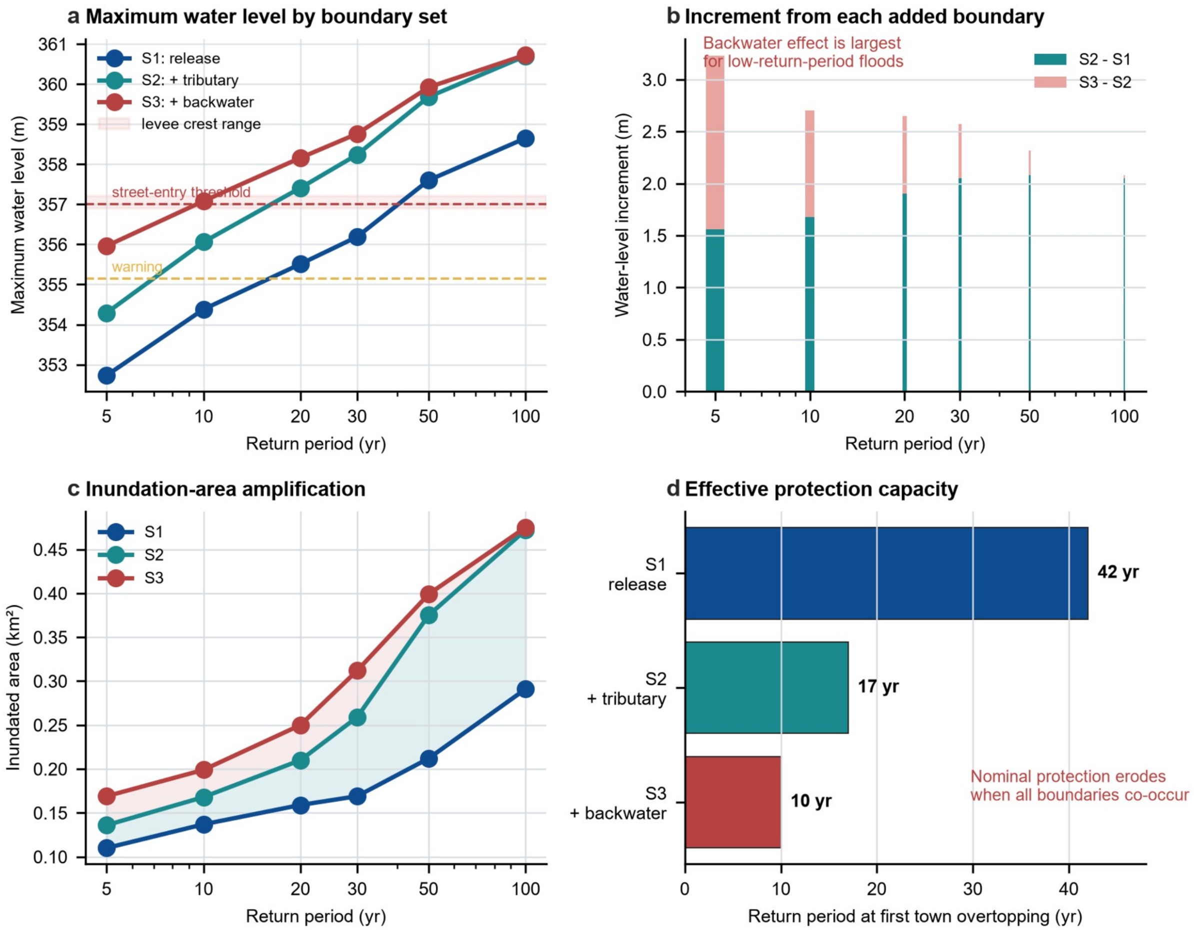

Figure 6. Multi-boundary scenario attribution. (a) Maximum water level for S1–S3 across return periods, with local thresholds. (b) Incremental stage rise from the tributary and downstream backwater boundaries. (c) Inundation-area amplification under nested boundaries. (d) Effective protection capacity decreases from about 42 years under S1 to about 10 years under S3. All panels were newly drawn from the hydrodynamic simulations and threshold analysis conducted for the present study

https://doi.org/10.5194/egusphere-2026-4327
Preprint. Discussion started: 17 August 2026

Table 4. Multi-boundary scenario water levels and inundation areas. RP, return period; WL, water level; S1, mainstream-only boundary; S2, S1 plus Qiedao tributary inflow; S3, S2 plus Jinlongtan backwater; S3−S1 WL rise, total water-level rise from the mainstream-only to the full compound boundary.

RP (yr)	S1 WL (m)	S2 WL (m)	S3 WL (m)	S3−S1 WL rise (m)	S1 area (km²)	S2 area (km²)	S3 area (km²)
5	352.73	354.29	355.96	3.23	0.110	0.136	0.169
10	354.38	356.06	357.08	2.70	0.137	0.168	0.199
20	355.51	357.41	358.16	2.65	0.159	0.210	0.250
30	356.19	358.24	358.76	2.57	0.169	0.259	0.312
50	357.60	359.68	359.92	2.32	0.212	0.375	0.399
100	358.65	360.70	360.73	2.08	0.291	0.472	0.475

5 Discussion

5.1 Mechanisms of engineering-induced flood-risk transformation

The results support a bounded explanation of recent risk escalation. They do not show that engineering change is the sole cause of every flood; rather, they show that upstream release, tributary inflow, and downstream stage can jointly move the town across impact thresholds that would not be crossed under the mainstream-only boundary. The 42-to-17-to-10-year sequence is therefore a hydraulic expression of altered practical protection, not a universal redesign standard.

The reservoir results should not be interpreted as evidence that regulation is intrinsically harmful. Najitan reduced the 2023 peak, and the levee limits direct overflow below its crest. The residual risk arises from system coupling: a high or sustained regulated release can still coincide with Qiedao inflow, while the Jinlongtan stage reduces the downstream gradient. The modelled tributary increment persists across the return-period range, whereas the marginal backwater effect is largest for frequent-to-moderate floods.

This return-period dependence explains why a downstream impoundment boundary can be operationally important even when its incremental effect becomes small during extreme floods. At lower return periods, a 1–2 m stage increment can determine whether water remains within the river corridor or enters streets and public-service locations. At higher return periods, the natural flood stage is already dominant, so the same downstream control contributes a smaller marginal increment.

Levee and drainage evidence identifies a second interaction pathway. The defended riverfront can remain vulnerable to internal runoff and backflow when the receiving river is high. The project calculations give a design drainage demand of about 2.62 $m^3 s^{-1}$, a recommended pump capacity of 3.0 $m^3 s^{-1}$, and an inlet-culvert capacity of about 3.68 $m^3 s^{-1}$. These flows are small relative to the river discharge but can control whether water leaves the low-lying protected area.

Exposure change can amplify the consequences of these hydraulic shifts. The 2009–2023 image comparison is consistent with denser occupation of the riverfront and confluence lowland, but the absence of harmonized building-footprint vectors prevents a quantitative attribution of exposure growth. Climate variability, reporting change, sedimentation, vegetation, and channel modification also remain plausible contributors. The most defensible interpretation is therefore a coupled transformation of hydraulic boundaries, drainage conditions, and exposure, with unequal evidence strength for each component.

5.2 Implications for compound-flood risk management in historic mountain towns

Baifusi extends compound-flood reasoning to a mountainous engineered basin. The interacting controls are not coastal surge and tide but reservoir release, tributary inflow, downstream backwater, local runoff, drainage state, and exposure. This combination makes a single rainfall total or upstream discharge gauge insufficient for impact-based warning.

Operational monitoring should therefore combine Najitan inflow, pool level and release, Qiedao flow and timing, Jinlongtan stage, local rainfall, and drainage-gate or pump status. Forecasts can then identify whether an approaching event is mainstream-dominated, tributary-dominated, backwater-dominated, drainage-limited, or compound, and compare the predicted stage directly with street-entry and public-service thresholds.

For reservoir operation, the appropriate objective is coordinated boundary management rather than independent single-reservoir peak reduction. Candidate measures include pre-release at Najitan when forecast uncertainty permits, avoiding coincidence between Najitan release and the Qiedao peak, and coordinating Jinlongtan drawdown or gate opening to reduce tailwater during the critical town-stage window. Each option requires testing against reservoir-safety, power-generation, and downstream constraints before operational adoption.

Structural measures should be evaluated as linked packages. Levee upgrading without drainage improvement can transfer risk from direct overflow to internal ponding; downstream conveyance works without exposure control can encourage further occupation of residual-risk areas. Backflow gates, pump completion, outlet maintenance, confluence-stage triggers, and restrictions or adaptive retrofitting in low-lying heritage zones should therefore be assessed together (Table 5).

https://doi.org/10.5194/egusphere-2026-4327
Preprint. Discussion started: 17 August 2026

This package shifts the management target from a nominal return-period defence to conditional threshold exceedance. Interpretable surrogate results can support rapid screening of terrain and hydrograph controls, but hydraulic scenarios remain the basis for evaluating engineering alternatives. The transferable element is the boundary-to-threshold workflow; the numerical thresholds and operation rules remain site specific. This integrated framing is consistent with urban-flood response approaches that link forcing, drainage, hydraulic routing, and exposure management (Pal et al., 2023).

Table 5. Mechanism-to-management translation for a compound flood-risk management system.

Mechanism	Evidence	Implication	Recommended action
Upstream release timing	2023 peak reduced from 4727.11 to 4000 $m^3 s^{-1}$ but high release persisted during compound conditions	Peak reduction alone does not guarantee town safety	Joint Najitan–Jinlongtan–Qiedao forecast and pre-release rules
Tributary coincidence	Adding Qiedao inflow to the mainstream-only condition lowers effective capacity from about 42 to 17 years	Qiedao is a threshold-control boundary	Add tributary monitoring, short-lead forecasting and confluence-stage triggers
Downstream backwater	Adding Jinlongtan backwater to the tributary-added condition lowers effective capacity to about 10 years; the 5-year backwater increment is about 1.67 m	Tailwater dominates frequent-to-moderate flood amplification	Review Jinlongtan gate capacity, opening timing and downstream conveyance
Levee-drainage side effect	Levee protects against external overflow but can obstruct mountain runoff and drainage outlets	Internal waterlogging and backflow must be managed with river stage	Backflow gates, pump-station completion, outlet checks and drainage-stage rules
Exposure expansion	imagery from 2009 and 2023 shows denser low-lying riverfront occupation	Engineering protection can encourage residual-risk accumulation	Floodplain zoning, building-floor elevation controls and relocation/retrofit options
Return-period blind spot	2023 local rainfall return periods were below 10 years, yet town inundation occurred	Single-driver design standards miss compound boundary states	Adopt compound grades integrating release, tributary flow, tailwater and drainage

5.3 Uncertainty, limitations, and research priorities

The scenario increments are deterministic model outputs rather than statistical confidence intervals. A diagnostic ±0.20 m band around the hospital-entrance threshold changes the interpolated capacity by about ±2.8 years for S1, ±1.5 years for S2, and ±0.9 years for S3. These ranges are smaller than the modelled shift from about 42 to 10 years, so the qualitative ordering of the scenarios is stable under moderate threshold uncertainty.

https://doi.org/10.5194/egusphere-2026-4327
Preprint. Discussion started: 17 August 2026

The historical frequency comparison is limited by small counts and heterogeneous records. County-wide mountain-flood disasters, rainfall warnings, flooded years, and town-level street-entry events are not fully harmonized, and recent events may be better documented. A year-by-year, consistently classified catalogue is needed before formal change-point or nonstationary-frequency analysis is justified.

Event-boundary reconstruction also contains unresolved source differences. The stand-alone Najitan file records a 4000 $m^3 s^{-1}$ release peak on 25 July 2023, whereas the integrated monitoring workbook records 4700 $m^3 s^{-1}$ later that day. Both indicate a high-release period close to the tributary and downstream peaks, but event-specific hydrograph inference remains provisional until the records are reconciled.

Exposure and drainage are less completely quantified than the hydraulic boundary effects. Building-footprint histories, floor elevations, levee-crest surveys, outlet and gate levels, pump-operation logs, and synchronized local-runoff observations would allow direct separation of exposure growth, drainage restriction, and external-river forcing. Until then, these pathways should be treated as locally supported amplifiers rather than fully quantified causal effects.

Model uncertainty remains in cross-section interpolation, floodplain elevation, roughness, lateral coupling, boundary timing, and the stage or rating representation at Jinlongtan. Qiedao lacks a long gauged series, and constant roughness does not represent possible stage-dependent resistance under backwater. Multiple parameter or structural representations can reproduce selected observations (Beven, 2006; Abbaszadeh et al., 2022), and scale transfer can bias hydraulic assessments (Hinkel et al., 2021). Future work should combine longer monitoring, dynamic roughness tests, ensemble boundary timing, and nonstationary scenario analysis.

6 Conclusions

This study presents the Baifusi case as a compound engineering-risk diagnosis rather than a simple flood-simulation study. The main conclusion is that the recent increase in damaging inundation is not explained by a monotonic increase in rainfall or by one reservoir alone. The best-supported explanation is the coupled influence of upstream release, Qiedao tributary timing and Jinlongtan downstream stage, amplified by levee-constrained drainage and expansion of buildings into low-lying riverfront zones. Under matched scenarios, the Qiedao tributary raises the maximum water level by 1.56–2.08 m across the 5–100-year range, whereas the marginal Jinlongtan backwater increment decreases from 1.67 m at 5 years to 0.03 m at 100 years. Relative to the 357.01 m hospital-entrance threshold, these boundary additions reduce effective protection capacity from about 42 years under S1 to 17 years under S2 and 10 years under S3.

Historical evidence supports this interpretation. The 2016 published analysis reported rare 24 h rainfall at Jinlongtan but only a moderate flood-peak return period at Najitan, and it already noted backwater effects. The 2023 event

https://doi.org/10.5194/egusphere-2026-4327
Preprint. Discussion started: 17 August 2026

provides a stronger calibration case: the floodmark elevation of 358.22 m nearly matches the monitored peak stage of 358.20 m, and floodmark-based peak estimates for 2016, 2020, 2021 and 2023 are broadly comparable.

Engineering records clarify the downstream boundary. Jinlongtan operation documents define 1500 and 3200 $m^3 s^{-1}$ rule thresholds and a 344.50 m control/normal-pool level. The 2023 log indicates rapid safety-oriented gate operation, including gate opening at 09:15 and five gates fully open by 11:33 on 25 July, with hourly spillway releases reaching about 5900 $m^3 s^{-1}$. This does not remove downstream influence; it shows why the downstream boundary must be modelled dynamically.

The exposure pathway is a plausible additional amplifier. Satellite images and field interpretation show that riverfront occupation intensified between 2009 and 2023, with dense buildings close to the levee and some former first-floor spaces becoming basement-like low-lying exposure. The drainage calculation shows a design drainage flow of only about 2.62 $m^3 s^{-1}$, so local rainfall and hillside runoff can become damaging when high river stage blocks gravity drainage.

For practice, the Baifusi problem should be managed through a multi-boundary risk-management system rather than by only raising a return-period design standard. Priority measures include integrated Najitan-Jinlongtan-Qiedao forecasting, dynamic gate-operation triggers tied to town-stage thresholds, backflow-safe drainage outlets and pumps, strict control of low-lying redevelopment, and explicit warning levels for internal drainage failure.

Further improvement of the evidence base would benefit from GIS building-footprint vectors, raw hydrodynamic boundary files, reconciled reservoir release hydrographs, pump-operation logs and a unified vertical-datum statement. These additions would allow exposure migration, drainage capacity and model uncertainty to be quantified more fully, but they do not change the main conclusion that compound engineering boundaries have lowered the effective threshold for damaging inundation.

Code and data availability

Processed data supporting the tables and figures can be made available by the corresponding author upon reasonable request. Raw hydrological records, reservoir-operation logs, DEM products, engineering-design files and local flood-control materials are not publicly deposited because they include local-government flood-control records and engineering-operation information subject to project and management restrictions. Access to these materials requires permission from the relevant data owners. No standalone model code is released with this manuscript; the hydraulic and machine-learning workflows are described in the Methods section and in the cited model-framework study.

https://doi.org/10.5194/egusphere-2026-4327
Preprint. Discussion started: 17 August 2026

Author contributions

Hairun Shu: Investigation, data curation and processing, formal analysis and modelling, and writing – original draft. Yi Liu: Conceptualization (manuscript-structure design). Jun Guo: Formal analysis (hydrological analysis). Miao Xiao: Methodology and formal analysis (hydraulic modelling and interpretability analysis). Zhenhan Deng: Formal analysis (reservoir-impact assessment).

Competing interests

The authors declare that they have no conflict of interest.

Disclaimer

Publisher's note: Copernicus Publications remains neutral with regard to jurisdictional claims in published maps and institutional affiliations.

Acknowledgements

The authors acknowledge the research materials, field observations, modelling datasets, and technical support of the project team. AI-assisted language editing was used to improve grammar, consistency, and document formatting; all scientific interpretation, data analysis, and final responsibility remain with the authors.

Financial support

This research has been supported by the National Key R&D Program of China (grant no. 2023YFC3209105), the Science and Technology Plan Project of Hubei Province (grant no. 2025BCA003), the National Natural Science Foundation of China (grant no. U2340211), and the Key Science and Technology Project of Water Conservancy in Hubei Province (grant no. HBSLKY202413).

References

Abbaszadeh, P., Munoz, D. F., Moftakhari, H., Jafarzadegan, K., and Moradkhani, H.: Perspective on uncertainty quantification and reduction in compound flood modeling and forecasting, iScience, 25, 105201, https://doi.org/10.1016/j.isci.2022.105201, 2022.

https://doi.org/10.5194/egusphere-2026-4327
Preprint. Discussion started: 17 August 2026

Alfieri, L., Libertino, A., Campo, L., Dottori, F., Gabellani, S., Ghizzoni, T., Masoero, A., Rossi, L., Rudari, R., Testa, N., Trasforini, E., Amdihun, A., Ouma, J., Rossi, L., Tramblay, Y., Wu, H., and Massabo, M.: Impact-based flood forecasting in the Greater Horn of Africa, Nat. Hazards Earth Syst. Sci., 24, 199-224, https://doi.org/10.5194/nhess-24-199-2024, 2024.

Apel, H., Aronica, G. T., Kreibich, H., and Thieken, A. H.: Flood risk analyses - how detailed do we need to be?, Nat. Hazards, 49, 79-98, https://doi.org/10.1007/s11069-008-9277-8, 2009.

Baifusi Project Team: Flood-safety investigation, hydrodynamic modelling, drainage calculation and reservoir-operation materials for Baifusi Town, internal technical dataset and reports, Laifeng County, Hubei Province, China, 2024.

Bates, P. D., Horritt, M. S., and Fewtrell, T. J.: A simple inertial formulation of the shallow water equations for efficient two-dimensional flood inundation modelling, J. Hydrol., 387, 33-45, https://doi.org/10.1016/j.jhydrol.2010.03.027, 2010.

Bates, P. D., Quinn, N., Sampson, C., Smith, A., Wing, O., Sosa, J., Savage, J., Olcese, G., Neal, J., Schumann, G., and others: Combined modeling of US fluvial, pluvial, and coastal flood hazard under current and future climates, Water Resour. Res., 57, e2020WR028673, https://doi.org/10.1029/2020WR028673, 2021.

Betterle, A. and Salamon, P.: Water depth estimate and flood extent enhancement for satellite-based inundation maps, Nat. Hazards Earth Syst. Sci., 24, 2817-2836, https://doi.org/10.5194/nhess-24-2817-2024, 2024.

Bevacqua, E., Maraun, D., Vousdoukas, M. I., Voukouvalas, E., Vrac, M., Mentaschi, L., and Widmann, M.: Higher probability of compound flooding from precipitation and storm surge in Europe under anthropogenic climate change, Sci. Adv., 5, eaaw5531, https://doi.org/10.1126/sciadv.aaw5531, 2019.

Bevacqua, E., Vousdoukas, M. I., Zappa, G., Hodges, K. I., Shepherd, T. G., Maraun, D., Mentaschi, L., and Feyen, L.: More meteorological events that drive compound coastal flooding are projected under climate change, Commun. Earth Environ., 1, 47, https://doi.org/10.1038/s43247-020-00044-z, 2020.

Bevacqua, E., Suarez-Gutierrez, L., Jezequel, A., Lehner, F., Vrac, M., Yiou, P., and Zscheischler, J.: Advancing research on compound weather and climate events via large ensemble model simulations, Nat. Commun., 14, 2145, https://doi.org/10.1038/s41467-023-37847-5, 2023.

Beven, K.: A manifesto for the equifinality thesis, J. Hydrol., 320, 18-36, https://doi.org/10.1016/j.jhydrol.2005.07.007, 2006.

Bloschl, G., Hall, J., Viglione, A., Perdigao, R. A. P., Parajka, J., Merz, B., Lun, D., Arheimer, B., Aronica, G. T., Bilibashi, A., and others: Changing climate both increases and decreases European river floods, Nature, 573, 108-111, https://doi.org/10.1038/s41586-019-1495-6, 2019.

Cea, L., Alvarez, M., and Puertas, J.: Using integrated hydrological-hydraulic modelling and global data sources to analyse the February 2023 floods in the Umbeluzi Catchment (Mozambique), Nat. Hazards Earth Syst. Sci., 24, 225-243, https://doi.org/10.5194/nhess-24-225-2024, 2024.

Davenport, F. V., Burke, M., and Diffenbaugh, N. S.: Contribution of historical precipitation change to US flood damages, Proc. Natl. Acad. Sci. U.S.A., 118, e2017524118, https://doi.org/10.1073/pnas.2017524118, 2021.

Devitt, L., Neal, J., Coxon, G., Savage, J., and Wagener, T.: Flood hazard potential reveals global floodplain settlement patterns, Nat. Commun., 14, 2801, https://doi.org/10.1038/s41467-023-38297-9, 2023.

Fowler, H. J., Lenderink, G., Prein, A. F., Westra, S., Allan, R. P., Ban, N., Barbero, R., Berg, P., Blenkinsop, S., Do, H. X., and others: Anthropogenic intensification of short-duration rainfall extremes, Nat. Rev. Earth Environ., 2, 107-122, https://doi.org/10.1038/s43017-020-00128-6, 2021.

Goulart, H. M. D., Benito Lazaro, I., van Garderen, L., van der Wiel, K., Le Bars, D., Koks, E., and van den Hurk, B.: Compound flood impacts from Hurricane Sandy on New York City in climate-driven storylines, Nat. Hazards Earth Syst. Sci., 24, 29-45, https://doi.org/10.5194/nhess-24-29-2024, 2024.

Grabowski, R., Vercruysse, K., Holman, I., Azhoni, A., Bala, B., and others: The land-river interface: a conceptual framework of environmental process interactions to support sustainable development, Sustain. Sci., 17, 1677-1693, https://doi.org/10.1007/s11625-022-01150-x, 2022.

Green, J., Haigh, I. D., Quinn, N., Neal, J., Wahl, T., Wood, M., Eilander, D., de Ruiter, M., Ward, P., and Camus, P.: Review article: A comprehensive review of compound flooding literature with a focus on coastal and estuarine regions, Nat. Hazards Earth Syst. Sci., 25, 747-816, https://doi.org/10.5194/nhess-25-747-2025, 2025.

Grodek, T. and Benito, G.: Reevaluating flood protection: disaster risk reduction for urbanized alluvial fans, Nat. Hazards Earth Syst. Sci., 25, 4343-4360, https://doi.org/10.5194/nhess-25-4343-2025, 2025.

Hinkel, J., Feyen, L., Hemer, M., Le Cozannet, G., Lincke, D., Marcos, M., Mentaschi, L., Merkens, J.-L., de Moel, H., Muis, S., and others: Uncertainty and bias in global to regional scale assessments of current and future coastal flood risk, Earth's Future, 9, e2020EF001882, https://doi.org/10.1029/2020EF001882, 2021.

Huang, X. and Swain, D. L.: Climate change is increasing the risk of a California megaflood, Sci. Adv., 8, eabq0995, https://doi.org/10.1126/sciadv.abq0995, 2022.

Jafarzadegan, K., Moradkhani, H., Pappenberger, F., Moftakhari, H., Bates, P., Abbaszadeh, P., Marsooli, R., Ferreira, C., Cloke, H. L., Ogden, F., and Duan, Q.: Recent advances and new frontiers in riverine and coastal flood modeling, Rev. Geophys., 61, e2022RG000788, https://doi.org/10.1029/2022RG000788, 2023.

Keller, K., Helgeson, C., and Srikrishnan, V.: Climate risk management, Annu. Rev. Earth Planet. Sci., 49, 95-116, https://doi.org/10.1146/annurev-earth-080320-055847, 2021.

https://doi.org/10.5194/egusphere-2026-4327
Preprint. Discussion started: 17 August 2026

Khosh Bin Ghomash, S., Apel, H., and Caviedes-Voullieme, D.: Are 2D shallow-water solvers fast enough for early flood warning? A comparative assessment on the 2021 Ahr valley flood event, Nat. Hazards Earth Syst. Sci., 24, 2857-2874, https://doi.org/10.5194/nhess-24-2857-2024, 2024.

Khosh Bin Ghomash, S., Yeste, P., Apel, H., and Nguyen, V. D.: Monte Carlo-based sensitivity analysis of the RIM2D hydrodynamic model for the 2021 flood event in western Germany, Nat. Hazards Earth Syst. Sci., 25, 975-990, https://doi.org/10.5194/nhess-25-975-2025, 2025.

Koks, E. E., Rozenberg, J., Zorn, C., Tariverdi, M., Vousdoukas, M., Fraser, S. A., Hall, J. W., and Hallegatte, S.: A global multi-hazard risk analysis of road and railway infrastructure assets, Nat. Commun., 10, 2677, https://doi.org/10.1038/s41467-019-10442-3, 2019.

Kreibich, H., Van Loon, A. F., Schraner, M., Ward, P. J., Mazzoleni, M., Sairam, N., Abeshu, G. W., Agafonova, S., AghaKouchak, A., Aksoy, H., and others: The challenge of unprecedented floods and droughts in risk management, Nature, 608, 80-86, https://doi.org/10.1038/s41586-022-04917-5, 2022.

Mazzoleni, M., Dottori, F., Cloke, H. L., and Di Baldassarre, G.: Deciphering human influence on annual maximum flood extent at the global level, Commun. Earth Environ., 3, 262, https://doi.org/10.1038/s43247-022-00598-0, 2022.

Merz, B., Bloschl, G., Vorogushyn, S., Dottori, F., Aerts, J. C. J. H., Bates, P., Bertola, M., Kemter, M., Kreibich, H., Lall, U., and Macdonald, E.: Causes, impacts and patterns of disastrous river floods, Nat. Rev. Earth Environ., 2, 592-609, https://doi.org/10.1038/s43017-021-00195-3, 2021.

Merz, B., Bloeschl, G., Juepner, R., Kreibich, H., Schroeter, K., and Vorogushyn, S.: Invited perspectives: safeguarding the usability and credibility of flood hazard and risk assessments, Nat. Hazards Earth Syst. Sci., 24, 4015-4030, https://doi.org/10.5194/nhess-24-4015-2024, 2024.

Montanari, A., Merz, B., and Bloeschl, G.: HESS Opinions: The sword of Damocles of the impossible flood, Hydrol. Earth Syst. Sci., 28, 2603-2615, https://doi.org/10.5194/hess-28-2603-2024, 2024.

Pal, L., Saksena, S., Dey, S., Merwade, V., and Ojha, C. S. P.: An integrative framework for assessment of urban flood response to changing climate, Water Resour. Res., 59, e2023WR034466, https://doi.org/10.1029/2023WR034466, 2023.

Pregnolato, M., Ford, A., Wilkinson, S. M., and Dawson, R. J.: The impact of flooding on road transport: a depth-disruption function, Transp. Res. Part D Transp. Environ., 55, 67-81, https://doi.org/10.1016/j.trd.2017.06.020, 2017.

Rentschler, J., Salhab, M., and Jafino, B. A.: Flood exposure and poverty in 188 countries, Nat. Commun., 13, 3527, https://doi.org/10.1038/s41467-022-30727-4, 2022.

Rhein, B. and Kreibich, H.: Causes of the exceptionally high number of fatalities in the Ahr valley, Germany, during the 2021 flood, Nat. Hazards Earth Syst. Sci., 25, 581-589, https://doi.org/10.5194/nhess-25-581-2025, 2025.

https://doi.org/10.5194/egusphere-2026-4327
Preprint. Discussion started: 17 August 2026

Sampson, C. C., Smith, A. M., Bates, P. D., Neal, J. C., Alfieri, L., and Freer, J. E.: A high-resolution global flood hazard model, Water Resour. Res., 51, 7358-7381, https://doi.org/10.1002/2015WR016954, 2015.

Schlef, K. E., Kunkel, K. E., Brown, C., Demissie, Y., Lettenmaier, D. P., Wagner, A., Wigmosta, M. S., Karl, T. R., Easterling, D. R., Wang, K. J., and others: Incorporating non-stationarity from climate change into rainfall frequency and intensity-duration-frequency (IDF) curves, J. Hydrol., 616, 128757, https://doi.org/10.1016/j.jhydrol.2022.128757, 2023.

Slater, L. J., Anderson, B., Buechel, M., Dadson, S., Han, S., Harrigan, S., Kelder, T., Kowal, K., Lees, T., Matthews, T., and others: Nonstationary weather and water extremes: a review of methods for their detection, attribution, and management, Hydrol. Earth Syst. Sci., 25, 3897-3935, https://doi.org/10.5194/hess-25-3897-2021, 2021a.

Slater, L. J., Villarini, G., and Bradley, A. A.: Global changes in 20-year, 50-year, and 100-year river floods, Geophys. Res. Lett., 48, e2020GL091824, https://doi.org/10.1029/2020GL091824, 2021b.

Song, L., Zhou, J., Guo, J., Zou, Q., and Liu, Y.: A robust well-balanced finite volume model for shallow water flows with wetting and drying over irregular terrain, Adv. Water Resour., 34, 915-932, https://doi.org/10.1016/j.advwatres.2011.04.017, 2011.

Tellman, B., Sullivan, J. A., Kuhn, C., Kettner, A. J., Doyle, C. S., Brakenridge, G. R., Erickson, T. A., and Slayback, D. A.: Satellite imaging reveals increased proportion of population exposed to floods, Nature, 596, 80-86, https://doi.org/10.1038/s41586-021-03695-w, 2021.

Wasko, C., Westra, S., Nathan, R., Pepler, A., Raupach, T. H., Dowdy, A., Johnson, F., Ho, M., McInnes, K. L., Jakob, D., and others: A systematic review of climate change science relevant to Australian design flood estimation, Hydrol. Earth Syst. Sci., 28, 1251-1285, https://doi.org/10.5194/hess-28-1251-2024, 2024.

Wing, O. E. J., Lehman, W., Bates, P. D., Sampson, C. C., Quinn, N., Smith, A. M., Neal, J. C., Porter, J. R., and Kousky, C.: Inequitable patterns of US flood risk in the Anthropocene, Nat. Clim. Change, 12, 156-162, https://doi.org/10.1038/s41558-021-01265-6, 2022.

Xiao, M., Shu, H., Liu, Y., Guo, J., Li, S., Cheng, C., Hu, H., Deng, Z., and Peng, X.: An interpretable adaptive mountain flood forecasting agent model framework based on multi-source terrain data, Engineering Applications of Computational Fluid Mechanics, 20, 2664290, https://doi.org/10.1080/19942060.2026.2664290, 2026.

Zscheischler, J., Westra, S., van den Hurk, B. J. J. M., Seneviratne, S. I., Ward, P. J., Pitman, A., AghaKouchak, A., Bresch, D. N., Leonard, M., Wahl, T., and Zhang, X.: Future climate risk from compound events, Nat. Clim. Change, 8, 469-477, https://doi.org/10.1038/s41558-018-0156-3, 2018.